Three-terminal refrigerator based on resonant-tunneling quantum wells

Zebin Lin, Yun Yun Yang, Wei Li, Jianghui Wang, and Jizhou He*
Department of Physics, Nanchang University, Nanchang 330031, People's Republic of China

(Received 7 July 2019; revised manuscript received 25 November 2019; accepted 18 January 2020; published 13 February 2020)

A three-terminal refrigerator based on resonant-tunneling quantum wells is proposed. With the help of the Landauer formula, the expressions for the cooling rate and the coefficient of performance (COP) are derived. The working regions of the refrigerator are determined and the three-dimensional projection graphs of the cooling rate and the COP varying with the positions of the two energy levels are plotted. Moreover, the influence of the bias voltage, the asymmetric factor, and the temperature difference on the optimal performance parameters is analyzed in detail. Finally, the performance characteristics of the refrigerator in the case of negative temperature difference are discussed.

DOI: 10.1103/PhysRevE.101.022117

I. INTRODUCTION

Thermoelectric devices can be used as power generators to convert heat to electricity based on the Seebeck effect or as refrigerators to cool a spatial region by external electricity based on the Peltier effect. With the development of nanotechnology there has been great interest in investigating highly efficient and powerful three-terminal nanoscale thermoelectric devices [1,2]. Compared with two-terminal setups, three-terminal ones can rectify thermal fluctuations from the hot reservoir and drive a directed charge current, can spatially separate the hot and cold reservoirs, and also exhibit a crossed flow of charge and heat currents.

For example, Edwards *et al.* investigated theoretically the quantum-dot refrigerator (QDR) which utilizes the discrete energy levels of quantum dots to customize the electronic Fermi-Dirac distribution, cooling a small reservoir to far below the ambient temperature [3,4]. Prance *et al.* presented experimental measurements of a QDR designed to cool a 6-μm^2 electron gas, and significant electrostatic interactions were observed in this device [5]. Later, Jordan *et al.* proposed a three-terminal heat engine with resonant-tunneling dots and obtained the maximum power and the corresponding efficiency [6]. Kano and Fujii studied the conversion efficiency of an energy harvester based on resonant tunneling through quantum dots in which heat leakage current from a hot reservoir to a cold reservoir is taken into account in the analysis of the harvester operation [7]. Sothmann *et al.* proposed a three-terminal heat engine based on resonant-tunneling wells and obtained the maximum power and the corresponding efficiency [8]. Choi and Jordan analyzed the performance of a three-terminal heat engine for energy harvesting and a refrigerator for cooling purposes based on semiconductor superlattices in which the periodicity of the superlattice structure creates an energy miniband; they also discussed phonon heat current through the system [9]. Other three-terminal thermoelectric devices with energy selective tunnels or ideal resonant-tunneling quantum dots have been extensively studied in the past several years [10–13]. Three- and multiterminal thermoelectric devices based on capacitively coupled quantum dots in the Coulomb-blockade regime theoretically [14–20] and experimentally [21–25] have been investigated. Three-terminal thermoelectric devices which are driven by phonons, magnons, and photons, have been analyzed [26–36].

On the basis of the previous works, we propose a three-terminal refrigerator based on resonant-tunneling quantum wells. It should be pointed out that the refrigeration model proposed here is not only the reverse operation of the energy harvester described in Ref. [8] but also includes the general expressions for charge and heat currents in linear response which may be directly used to discuss the optimal performance parameters and the critical temperature difference. The main focus in this paper is to analyze the thermodynamic performance characteristics and the optimal performance of a three-terminal quantum well refrigerator. The influence of the main parameters, including the positions of the two energy levels, bias voltage, asymmetry factor, and temperature difference on the refrigerator performance is discussed in detail.

This paper is organized as follows. In Sec. II, we briefly describe the model and basic physical theory of a three-terminal quantum well refrigerator and derive the general expressions for the cooling rate and the coefficient of performance (COP) based on the Landauer formula. In Sec. III, we analyze the working regions and the performance characteristics of the refrigerator. In Sec. IV, we investigate the optimal performance of the refrigerator. The influence of the bias voltage, asymmetry factor, and temperature difference on the optimal performance parameters is discussed in detail. In Sec. V, the performance characteristics of the refrigerator operated in cases of $\Delta T/T > 0$ and $\Delta T/T < 0$ are compared where ΔT is the temperature difference between the central cavity and the left and right electron reservoirs. Finally, the important results of this paper are summarized in Sec. VI.

*hjzhou@ncu.edu.cn

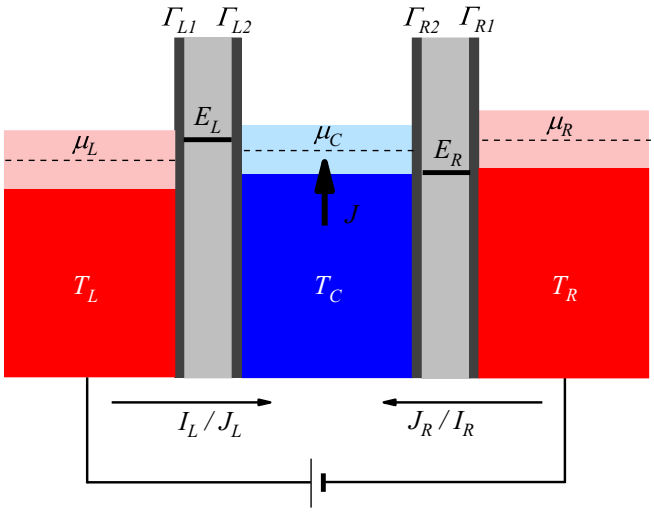

FIG. 1. Schematic diagram of a three-terminal refrigerator based on quantum well. A central cavity with temperature T_C and chemical potential μ_C is connected to the left and right electron reservoirs with temperature T_i ($i = L, R$) and chemical potential μ_i via quantum wells. The positive direction of charge and heat currents is indicated by arrows.

II. MODEL AND THEORY

The model we consider is schematically illustrated in Fig. 1. It consists of a central cavity connected via quantum wells to left and right electron reservoirs with temperature T_i ($i = L, R$). The central cavity is kept at temperature T_C by a cold thermal reservoir. The temperatures of the left and right reservoirs are the same and higher than that of the central cavity ($T_L = T_R > T_C$). When no bias voltage is applied, the chemical potential of the left electron reservoir is equal to the chemical potential of the right ($\mu_L = \mu_R = \mu_0$). When a bias voltage V is applied, we take $\mu_L = \mu_0 - 1/2eV$ and $\mu_R = \mu_0 + 1/2eV$ (e is the electronic charge). For simplicity, we take $\mu_0 = 0$ in numerical calculation. The chemical potential μ_C of the cavity is determined by the conservation of charge current, i.e., $I_L + I_R = 0$. The positive direction of charge and energy currents is flowing from the reservoir i into the cavity.

Based on the Landauer formula, the charge and energy currents flowing from the reservoir i into the cavity can be evaluated [8],

$$I_i = \frac{em^*A}{2\pi^2\hbar^3}\iint dE_\perp dE_Z \tau_i(E_Z)[f_i(E_Z + E_\perp) - f_C(E_Z + E_\perp)], \tag{1}$$

and

$$J_i = \frac{m^*A}{2\pi^2\hbar^3}\iint dE_\perp dE_Z (E_Z + E_\perp)\tau_i(E_Z)[f_i(E_Z + E_\perp) - f_C(E_Z + E_\perp)], \tag{2}$$

where $f_i = \{\exp[(E_Z + E_\perp - \mu_i)/k_BT_i] + 1\}^{-1}$ is the Fermi distribution of the reservoir i, $f_C = \{\exp[(E_Z + E_\perp - \mu_C)/k_BT_C] + 1\}^{-1}$ is the Fermi distribution of the cavity, E_Z is the component of electron energy parallel to the direction of transport, $E_\perp$ is the component of electron energy perpendicular to it, k_B is the Boltzmann constant, m^* is the effective electron mass, A is the surface area of the quantum well, and $\hbar$ is Planck's constant. $\tau_i(E_Z)$ is the transmission function of the quantum well i which is given by

$$\tau_i(E_Z) = \frac{\Gamma_{i1}(E_Z)\Gamma_{i2}(E_Z)}{(E_Z - E_i)^2 + [\Gamma_{i1}(E_Z) + \Gamma_{i2}(E_Z)]^2/4}, \tag{3}$$

where E_i is the energy of the resonant level within the quantum well i; Γ_{i2} and Γ_{i1} are the coupling strengths of the quantum well i to the cavity and the reservoir i, respectively.

To simplify notation, we introduce the temperature difference $\Delta T = T_i - T_C$ and average temperature $T = (T_C + T_i)/2$. In linear response, the temperature difference ΔT and chemical potential difference $\Delta\mu = \mu_R - \mu_L = eV$ are small. With the conservation of charge and energy in the cavity, i.e., $I_L + I_R = 0$ and $J_L + J_R + J = 0$, the net current flowing through the system, $I \equiv I_L = -I_R$, is given by

$$I = GV + GS(-\Delta T), \tag{4}$$

and the heat current injected from the cold thermal reservoir, $J = -J_L - J_R$, is given by (the detailed derivation is in the Appendix)

$$J = G\Pi V + (K + GS\Pi)(-\Delta T), \tag{5}$$

where G, S, and K are the electrical conductance, the Seebeck coefficient, and the thermal conductance, respectively; Π is the Peltier coefficient which is equal to $\Pi = -ST$ based on the Onsager reciprocal relation.

To linear order in the temperature difference ΔT and chemical potential difference eV, the expressions for these coefficients are given by

$$G = -\frac{e^2m_*A}{2\pi^2\hbar^3}\frac{G_{L1}G_{R1}}{G_{L1} + G_{R1}}, \tag{6}$$

$$S = \frac{k_B}{e}\left[\frac{G_{L2} + G_{L3}}{G_{L1}} - \frac{G_{R2} + G_{R3}}{G_{R1}}\right], \tag{7}$$

$$K = \frac{m_*A}{2\pi^2\hbar^3}k_B^2T\left[(G_{L4} + 2G_{L5} - 2G_{L6}) + (G_{R4} + 2G_{R5} - 2G_{R6}) - \frac{(G_{R2} + G_{R3})^2}{G_{R1}} - \frac{(G_{L2} + G_{L3})^2}{G_{L1}}\right], \tag{8}$$

$$\Pi = \frac{k_BT}{e}\left[\frac{G_{R2} + G_{R3}}{G_{R1}} - \frac{G_{L2} + G_{L3}}{G_{L1}}\right] = -ST, \tag{9}$$

with the auxiliary functions

$$G_{i1} = \int_{-\infty}^{\infty} dE_Z \tau_i(E_Z)\frac{1}{1 + e^{E_Z/k_BT}}, \tag{10}$$

$$G_{i2} = \int_{-\infty}^{\infty} dE_Z \tau_i(E_Z)\frac{E_Z/k_BT}{1 + e^{E_Z/k_BT}}, \tag{11}$$

$$G_{i3} = \int_{-\infty}^{\infty} dE_Z \tau_i(E_Z)\log(1 + e^{-E_Z/k_BT}), \tag{12}$$

$$G_{i4} = \int_{-\infty}^{\infty} dE_Z \tau_i(E_Z)\frac{(E_Z/k_BT)^2}{1 + e^{E_Z/k_BT}}, \tag{13}$$

$$G_{i5} = \int_{-\infty}^{\infty} dE_Z \tau_i(E_Z)(E_Z/k_BT)\log(1 + e^{-E_Z/k_BT}), \tag{14}$$

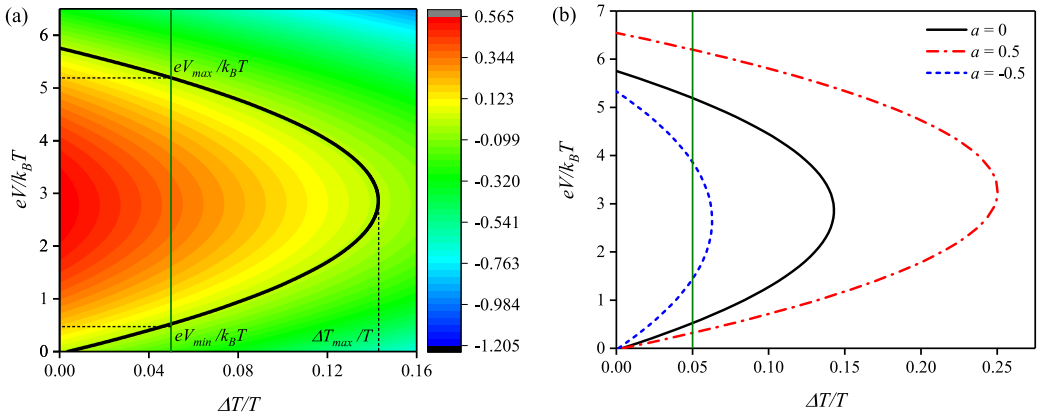

FIG. 2. (a) The three- dimensional projection of the cooling rate versus the temperature difference $\Delta T/T$ and the bias voltage eV for given $a = 0$. Panel (b) shows the working regions of the refrigerator for different asymmetry factors a. For both plots, $E_L = 1k_BT$ and $E_R = -5k_BT$.

$$G_{i6} = \int_{-\infty}^{\infty} dE_Z \tau_i(E_Z) \mathrm{Li}_2(-e^{-E_Z/k_BT}), \tag{15}$$

where we have introduced the integral $\mathrm{Li}_2(-e^z) = -\int_0^\infty t(1+e^{t-z})^{-1}dt$ with the dilogarithm $\mathrm{Li}_2(x) = \sum_{k=1}^{\infty}(x^k/k^2)$.

The electrical conductance shows that $G_{L1}(G_{R1})$ is proportional to the electrical conductance of the left (right) quantum well, so the net conductance G is simply the series combination of the two conductors. The three-terminal Seebeck coefficient S is determined by the difference between the left and right two-terminal Seebeck coefficient of each quantum well. Therefore, S depends on the properties of left and right quantum wells. When the left and right quantum wells are symmetrical, i.e., $\frac{G_{L2}+G_{L3}}{G_{L1}} = \frac{G_{R2}+G_{R3}}{G_{R1}}$, the Seebeck coefficient S vanishes; $S = 0$.

Eqation (5) shows that the first part is simply proportional to the charge current and the second part is the heat current generated by the temperature difference. The Peltier coefficient Π shows the presence of the heating from the Peltier contribution. The relation $\Pi = -ST$ shows that Π can be considered as the back action counterpart to S; the minus sign

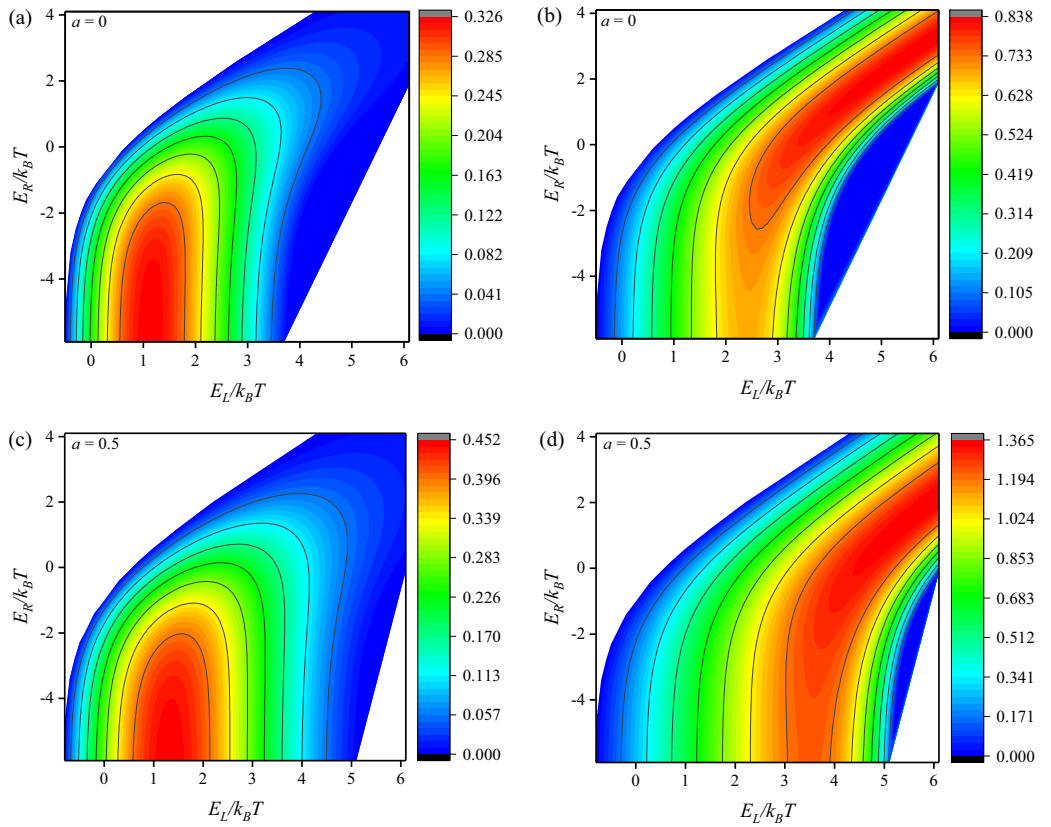

FIG. 3. (a), (c) The cooling rate $\dot{Q}_C$ versus the level positions (E_L, E_R) at different asymmetry factors a. (b), (d) The COP ε versus the level positions (E_L, E_R) at different asymmetry factors a. All plots are obtained for given $\Delta T/T = 0.05$ and $eV = 2k_BT$.

of the relation occurs because J is the heat current injected from the cold thermal reservoir into the cavity. This relation shows that our system satisfies Onsager symmetry resulting from the time reversibility.

It is easily seen from Eq. (5) that there exists a critical temperature difference $\Delta T_{\rm cri}$ for $J = 0$,

$$\Delta T_{\rm cri} = \frac{G\Pi}{K + GS\Pi} V. \tag{16}$$

It is a function of the bias voltage and the resonant-energy level. The refrigerator works only when the heat current is emitted by the cavity into the reservoirs, $J \geqslant 0$. Hence, the temperature reduction of the cavity should be in the range of $0 \leqslant \Delta T \leqslant \Delta T_{\rm cri}$.

We assume that the couplings are very weak, i.e., $\Gamma_{i1} = \Gamma_{i2} = \Gamma_i \ll k_B T_i,\ k_B T_C$; then the transmission function can be denoted as a delta function $\tau_i(E_Z) = \pi\,\Gamma_i\,\delta(E_Z - E_i)$. The expressions (1) and (2) for the charge and energy currents can be rewritten as

$$I_i = \frac{e m_* A}{2\pi\hbar^3}\Gamma_i\left[k_B T_i \xi\left(\frac{\mu_i - E_i}{k_B T_i}\right) - k_B T_C \xi\left(\frac{\mu_C - E_i}{k_B T_C}\right)\right], \tag{17}$$

and

$$J_i = \frac{E_i}{e} I_i + \frac{m_* A}{2\pi\hbar^3}\Gamma_i\left[(k_B T_i)^2 \phi\left(\frac{\mu_i - E_i}{k_B T_i}\right) - (k_B T_C)^2 \phi\left(\frac{\mu_C - E_i}{k_B T_C}\right)\right], \tag{18}$$

with the auxiliary functions $\xi(x) = \log(1 + e^x)$ and $\phi(x) = -\mathrm{Li}_2(-e^x)$.

Based on Eqs. (4) and (5) or (17) and (18) and the law of energy conservation in the cavity, the cooling rate is given by

$$\dot{Q}_C \equiv J = -J_L - J_R. \tag{19}$$

The input electrical power is $P = IV$. The coefficient of performance (COP) is given by

$$\varepsilon = \dot{Q}_C / P. \tag{20}$$

In the following, we assume the asymmetry between the coupling strengths of the left and right quantum wells, i.e., $\Gamma_L = (1 + a)\,\Gamma$, $\Gamma_R = (1 - a)\,\Gamma$, where a satisfies the bounds $-1 < a < 1$, and Γ is the total coupling strength. The cooling rate $\dot{Q}_C$ and the input electrical power P are in units of $\frac{m^* A\Gamma}{2\pi\hbar^3}(k_B T)^2$.

III. PERFORMANCE CHARACTERISTICS

Now we consider the working regions of the refrigerator at first. The three- dimensional projection of the cooling rate $\dot{Q}_C$ varying with the temperature difference $\Delta T/T$ and the bias voltage eV at symmetric case $a = 0$ for given $E_L = 1k_B T$ and $E_R = -5k_B T$ is shown in Fig. 2(a). The black curve in Fig. 2(a) represents when the cooling rate becomes zero. The left region of the curve is the working region of the refrigerator (i.e., $\dot{Q}_C > 0$ and $P > 0$). It is seen in Fig. 2(a) that the bias voltage has a start value $eV_{\rm min}$ and a stopping voltage $eV_{\rm max}$ when the temperature difference $\Delta T/T$ is given, and the temperature difference has a maximum value $\Delta T_{\rm max}/T$. The cooling regions for different asymmetry factors a are plotted as shown in Fig. 2(b). It is found that the working region increases as the asymmetry factor increases.

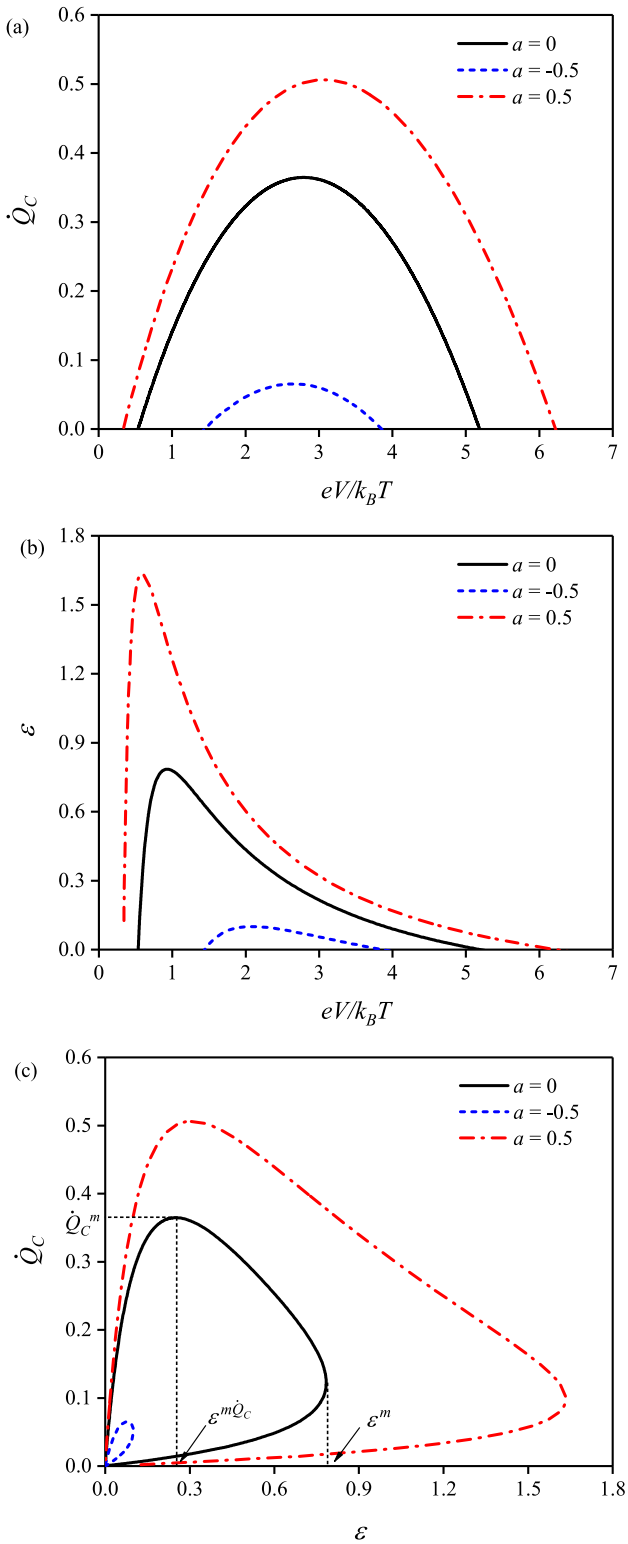

FIG. 4. (a) The cooling rate $\dot{Q}_C$ and (b) the COP ε versus the bias voltage eV at different asymmetry factors a. (c) The characteristic curves at different asymmetry factors a. All plots are obtained for given $\Delta T/T = 0.05$, $E_L = 1k_B T$, and $E_R = -5k_B T$.

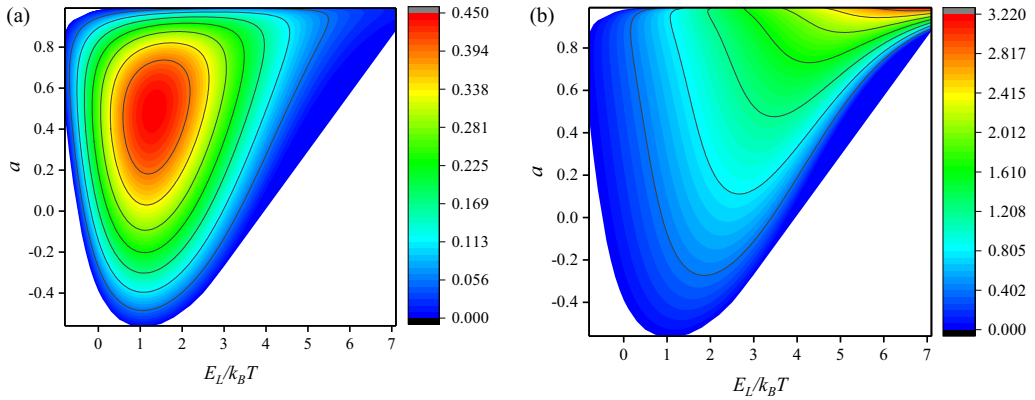

FIG. 5. (a),(b) The three- dimensional projections of the cooling rate and the COP varying with E_L and a for given $\Delta T/T = 0.05$, $eV = 2k_BT$, and $E_R = -5k_BT$, respectively.

According to Eqs. (17)–(20), we plot three- dimensional (3D) projection graphs of the cooling rate $\dot{Q}_C$ and the COP ε varying with the positions of the two energy levels E_L and E_R at different asymmetry factors a for given $\Delta T/T = 0.05$ and $eV = 2k_BT$, as shown in Fig. 3. It is seen from Fig. 3 that both the cooling rate and COP at $a = 0.5$ are larger than those at $a = 0$. In Figs. 3(a) and 3(c), the maximum cooling rate appears approximately at $E_L \approx 1k_BT$ and $E_R \approx -5k_BT$, and there exists an optimum energy level leading to a maximum cooling rate. However, the COP increases as the energy levels E_L and E_R increase, as shown in Figs. 3(b) and 3(d).

Similarly we plot the curves of the cooling rate $\dot{Q}_C$ and the COP ε versus the bias voltage eV at different asymmetry factors a for given $\Delta T/T = 0.05$, $E_L = 1k_BT$, and $E_R = -5k_BT$, as shown in Fig. 4. It is seen in Fig. 4(a) that the cooling rate first increases and then decreases as the bias voltage eV increases and is almost a symmetric parabolalike curve. However, the COP first increases rapidly and then decreases slowly as the bias voltage eV increases and is different from the curves of the cooling rate, as shown in Fig. 4(b). Especially, the characteristic curves of the cooling rate versus the COP are plotted, as shown in Fig. 4(c). It is

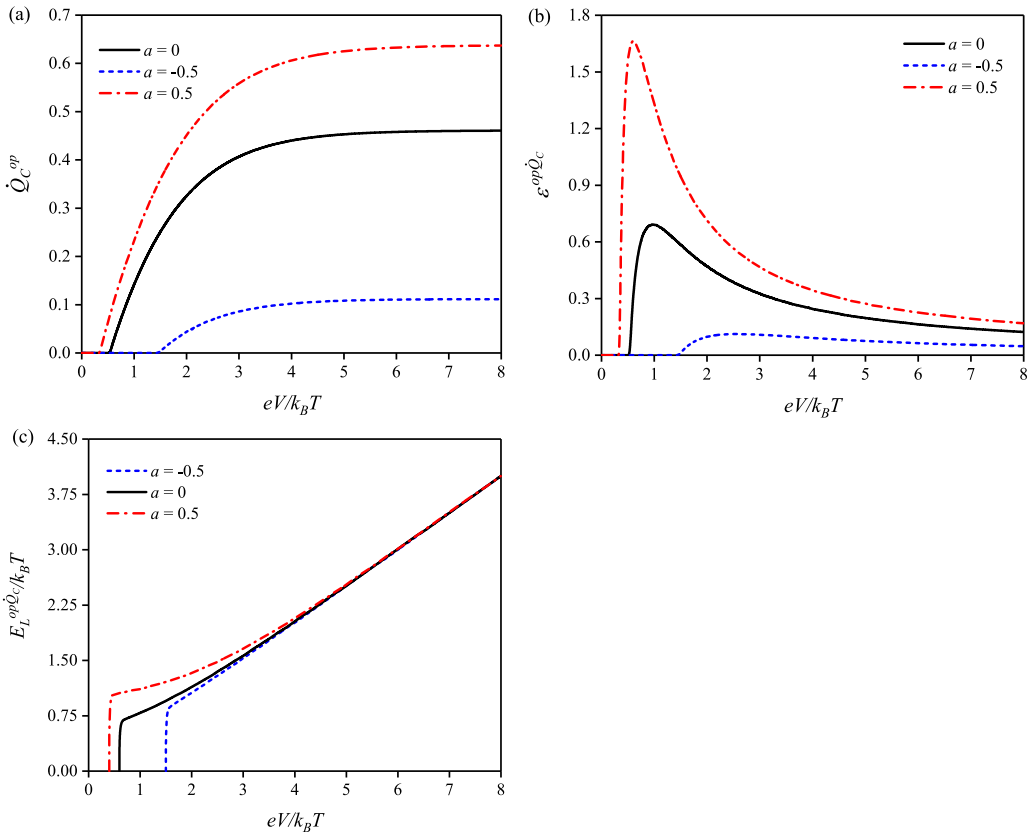

FIG. 6. (a) The optimized cooling rate $\dot{Q}_C^{op}$, (b) the corresponding COP $\varepsilon^{op\dot{Q}_C}$, and (c) the optimal position of left energy level $E_L^{op\dot{Q}_C}$ versus the bias voltage eV at different asymmetry factors a for given $\Delta T/T = 0.05$.

found that the characteristic curves between the cooling rate and the COP are the closed-loop-shaped ones. This means that the cooling power $\dot{Q}_c$ does not vanish at maximum COP condition. The refrigerator cannot operate in the reversible regime and the maximum value of the COP cannot achieve the Carnot COP $\varepsilon_C = T_C/(T_i - T_C) = T/\Delta T - 1/2$. The optimal operating regions of the refrigerator should be located in those of the $\dot{Q}_C \sim \varepsilon$ curves with a negative slope. The COP will decrease as the cooling rate increases, and vice versa. Thus the optimal ranges of the cooling rate and the coefficient of performance should satisfy

$$\dot{Q}_{C\varepsilon} \leqslant \dot{Q}_C \leqslant \dot{Q}_C^m, \tag{21}$$

$$\varepsilon_{mQ} \leqslant \varepsilon \leqslant \varepsilon^{\mathrm{m}}, \tag{22}$$

where $\dot{Q}_{C\varepsilon}$, $\dot{Q}_C^m$, ε_{mQ}, and ε^m are four important performance parameters which determine the lower and upper bounds of the optimal cooling rate and the coefficient of performance.

We now turn to the discussion of the cooling rate and COP at the asymmetry case. According to Eqs. (19) and (20), we plot 3D projection graphs of the cooling rate $\dot{Q}_C$ and the COP ε varying with the positions of the left energy levels E_L and the asymmetry factor a for given $\Delta T/T = 0.05$, $eV = 2k_BT$, and $E_R = -5k_BT$, as shown in Fig. 5. It is seen in Fig. 5(a) that the maximum cooling rate appears approximately at $E_L \approx 1.5k_BT$ and $a = 0.5$; there exists an optimum left energy level E_L and an optimum asymmetry factor leading to a maximum cooling rate. However, the COP increases as the left energy levels and the asymmetry factor increase, as shown in Fig. 5(b).

IV. PERFORMANCE OPTIMIZATION

Using Eqs. (19) and (20) and two partial differential equations,

$$\frac{\partial \dot{Q}_C}{\partial E_L} = 0 \quad \text{and} \quad \frac{\partial \dot{Q}_C}{\partial E_R} = 0, \tag{23}$$

we can numerically calculate the optimized cooling rate $\dot{Q}_C^{op}$ and the corresponding COP $\varepsilon^{op\dot{Q}_C}$. The curves of the optimized cooling rate and the corresponding COP at the optimized cooling rate are plotted as a function of the bias voltage eV at different asymmetry factors a for given $\Delta T/T = 0.05$, as shown in Fig. 6. It is seen in Fig. 6(a) that the optimized cooling rate is a monotonically increasing function of eV and has a saturation value at $eV \approx 8k_BT$. The corresponding COP at the optimized cooling rate first increases rapidly and then decreases to a saturation value as the bias voltage increases, as shown in Fig. 6(b). The optimal position of the left energy level $E_L^{op\dot{Q}_C}$ increases almost linearly with the bias voltage eV and $E_L^{op\dot{Q}_C} \approx 1/2eV$, as shown in Fig. 6(c). It is not shown in Fig. 6 that the optimal position of the right energy level $E_R^{op\dot{Q}_C}$ is a large negative value; i.e., $-E_R^{op\dot{Q}_C} \gg k_BT$. When the optimized cooling rate has a saturation value at $eV \approx 8k_BT$, the optimal position of the left energy level $E_L^{op\dot{Q}_C}$ is $E_L^{op\dot{Q}_C} \approx 4k_BT$.

Similarly, we plot the curves of the optimized cooling rate $\dot{Q}_C^{op}$ and the corresponding COP $\varepsilon^{op\dot{Q}_C}$ versus the asymmetry factor a for given $\Delta T/T = 0.05$ and the saturation bias voltage $eV \approx 8k_BT$, as shown in Fig. 7. It is seen in Fig. 7

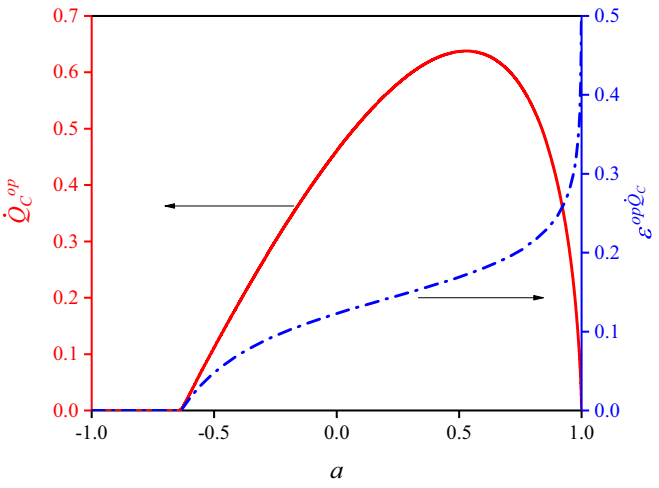

FIG. 7. The optimized cooling rate $\dot{Q}_C^{op}$ (solid) and the corresponding COP $\varepsilon^{op\dot{Q}_C}$ (dot dash) versus the asymmetry factor a for given $\Delta T/T = 0.05$ and $eV \approx 8k_BT$.

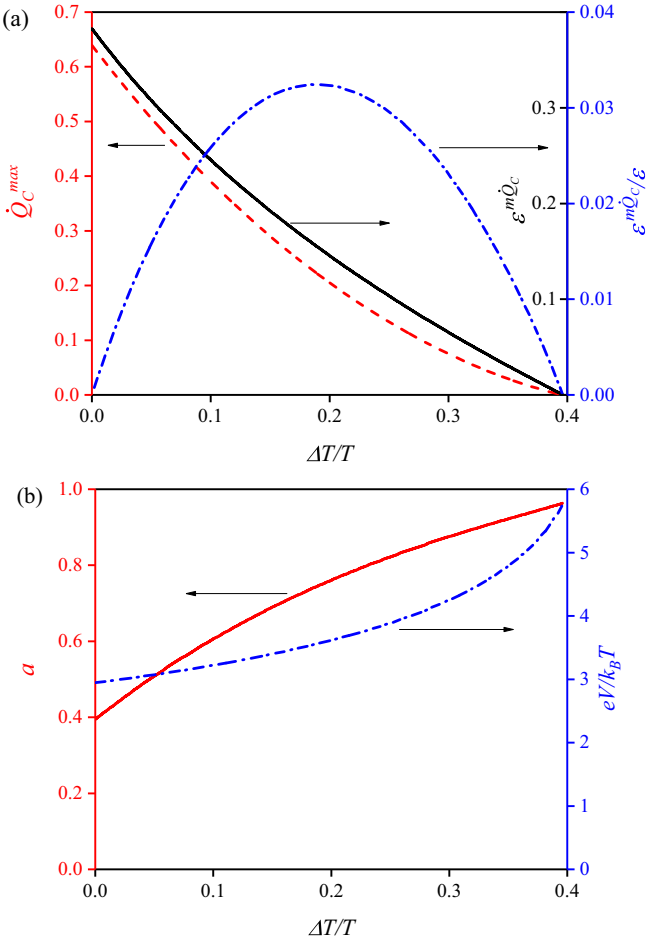

FIG. 8. (a) The maximum cooling rate $\dot{Q}_C^{\max}$ (dash) and the corresponding COP $\varepsilon^{m\dot{Q}_C}$ (solid) and the COP in units of Carnot COP $\varepsilon^{m\dot{Q}_C}/\varepsilon_C$ (dot dash) versus the temperature difference $\Delta T/T$. (b) The optimal asymmetry factor a (solid) and the optimal bias voltage eV (dot dash) versus the temperature difference $\Delta T/T$.

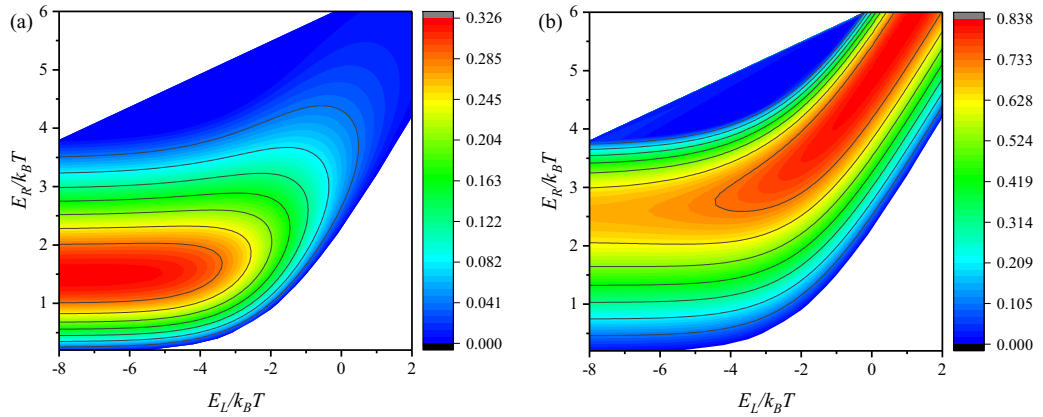

FIG. 9. The cooling rate (a) and COP (b) versus the level positions (E_L, E_R) for given $\Delta T/T = -0.05$, $eV = 2k_BT$, and $a = 0$.

that the optimized cooling rate $\dot{Q}_C^{op}$ first increases and then decreases as the asymmetry factor a increases and reaches its maximum at $a \approx 0.5$. The corresponding COP $\varepsilon^{op\dot{Q}_C}$ is a monotonically increasing function of the asymmetry factor a. In order to achieve the maximum cooling rate and at the same time obtain a large COP, the quantum well refrigerator should work in the region of $a \geqslant 0.5$. In the actual design, the optimal region of the asymmetry factor should be $0.5 \leqslant a \leqslant 1$.

In order to consider the influence of the temperature difference on the performance of the refrigerator, we maximize the cooling rate with respect to the bias voltage eV and the asymmetry factor a for the given positions of energy levels $E_L = 1k_BT$ and $E_R = -5k_BT$. Using Eqs. (19) and (20) and two partial differential equations,

$$\frac{\partial \dot{Q}_C}{\partial eV} = 0 \quad \text{and} \quad \frac{\partial \dot{Q}_C}{\partial a} = 0, \tag{24}$$

we can numerically calculate the maximum cooling rate $\dot{Q}_C^{\max}$, the corresponding COP at the maximum cooling rate $\varepsilon^{m\dot{Q}_C}$, the corresponding bias voltage eV, and the corresponding asymmetry factor a. The curves of the maximum cooling rate $\dot{Q}_C^{\max}$ (dash) and the corresponding COP at the maximum cooling rate $\varepsilon^{m\dot{Q}_C}$ (solid) are plotted as a function of the temperature difference $\Delta T/T$, as shown in Fig. 8(a). It is seen in Fig. 8(a) that the maximum cooling rate decreases as $\Delta T/T$ increases, and then vanishes at $\Delta T/T \approx 0.4$; the corresponding COP at the maximum cooling rate decreases as $\Delta T/T$ increases, and the corresponding COP in units of Carnot COP at the maximum cooling rate $\varepsilon^{\mathrm{m}\dot{Q}_C}/\varepsilon_C$ (dot dash) first increases and then decreases as $\Delta T/T$ increases and reaches its maximum value at $\Delta T/T \approx 0.2$. The optimal asymmetry factor a (solid) and the optimal bias voltage eV (dot dash) are plotted as a function of $\Delta T/T$ as shown in Fig. 8(b). It is seen in Fig. 8(b) that the asymmetry factor a and the bias voltage eV are the monotonically increasing function of $\Delta T/T$. Therefore, the refrigerator can be operated at the maximum cooling rate by reasonably choosing the asymmetry factor and the bias voltage for different $\Delta T/T$.

V. DISCUSSION AND COMPARISON

We turn to discuss the performance of the refrigerator operated in the case of $\Delta T/T < 0$; i.e., the cavity's temperature is higher than the reservoir's one. In this case, the heat current $\dot{Q}_i$ flows from the cavity into the thermal reservoir i into the cavity by the applied bias voltage. The energy current $-J$ is rejected to the thermal reservoir. According to the conservation of energy in the cavity, i.e., $\dot{Q}_i + J + P = 0$, the cooling rate is given by

$$\dot{Q}_i = -J - P, \tag{25}$$

and the COP is defined as

$$\varepsilon = \frac{\dot{Q}_i}{P} = \frac{-J - P}{P}. \tag{26}$$

According to Eqs. (25) and (26), we plot 3D projection graphs of the cooling rate $\dot{Q}_C$ and the COP ε varying with the positions of the two energy levels E_L and E_R for given $a = 0$, $\Delta T/T = -0.05$, and $eV = 2k_BT$, as shown in Fig. 9. It is seen in Fig. 9(a) that the maximum cooling rate appears approximately at $E_L \approx -5k_BT$ and $E_R \approx 1.5k_BT$. However, the COP increases with increase of the energy levels E_L and E_R as shown in Fig. 9(b). The result obtained in this case is similar to one in the case of $\Delta T/T > 0$ as long as the positions of the two energy levels E_L and E_R exchange each other.

VI. CONCLUSION

We have investigated the performance characteristics of a three-terminal refrigerator based on resonant-tunneling quantum wells, and have obtained the cooling region. Then, we have optimized the performance of the refrigerator and obtained these main results as follows: (1) the three-terminal quantum well refrigerator cannot operate in the reversible regime; (2) the performance of the refrigerator which works in the asymmetry case is better than that in the symmetry case; (3) the maximum cooling rate and the corresponding COP decrease as $\Delta T/T$ increases. The results obtained here can provide some theoretical guidelines for the design and operation of the practical quantum well refrigerators.

ACKNOWLEDGMENTS

This work has been supported by the National Natural Science Foundation (Grants No. 11875034 and No. 11365015), People's Republic of China. The authors acknowledge Andrew N. Jordan for insightful suggestions and comments on the manuscript.

APPENDIX

We here discuss the detailed derivation of Eqs. (4) and (5) in the main text.

$$
\begin{aligned}
I_i &= \frac{em_*A}{2\pi^2\hbar^3}\iint dE_\perp dE_Z \tau_i(E_Z)[f_i(E_Z+E_\perp)-f_C(E_Z+E_\perp)] \\
&= \frac{em_*A}{2\pi^2\hbar^3}\int dE_Z\tau_i(E_Z)\{kT_i\log[1+e^{(\mu_i-E_Z)/kT_i}]-kT_C\log[1+e^{(\mu_C-E_Z)/kT_C}]\} \\
&\approx \frac{em_*A}{2\pi^2\hbar^3}\int dE_Z\tau_i(E_Z)\left\{\frac{E_Z/kT}{1+e^{E_Z/kT}}k(T_i-T_C)+\log[1+e^{-E_Z/kT}]k(T_i-T_C)+\frac{1}{1+e^{E_Z/kT}}(\mu_i-\mu_C)\right\} \\
&= \frac{em_*A}{2\pi^2\hbar^3}\left\{\int dE_Z\tau_i(E_Z)\log[1+e^{-E_Z/kT}]k\Delta T+\int dE_Z\tau_i(E_Z)\frac{E_Z/kT}{1+e^{E_Z/kT}}k\Delta T+\int dE_Z\tau_i(E_Z)\frac{(\mu_i-\mu_C)}{1+e^{E_Z/kT}}\right\} \\
&= \frac{em_*A}{2\pi^2\hbar^3}[G_{i3}k\Delta T+G_{i2}k\Delta T+G_{i1}(\mu_i-\mu_C)], \\
&\quad \because I_L+I_R=0, \\
&\quad \therefore G_{L1}(\mu_L-\mu_C)+G_{R1}(\mu_R-\mu_C)+(G_{L2}+G_{L3}+G_{R2}+G_{R3})k\Delta T=0.
\end{aligned}
$$

$$
\mu_C = \frac{G_{L1}\mu_L+G_{R1}\mu_R+(G_{L2}+G_{L3}+G_{R2}+G_{R3})k\Delta T}{G_{L1}+G_{R1}},
$$

$$
\begin{aligned}
I_L &= \frac{em_*A}{2\pi^2\hbar^3}[G_{L1}(\mu_L-\mu_C)+(G_{L2}+G_{L3})k\Delta T] \\
&= \frac{em_*A}{2\pi^2\hbar^3}\left\{-\frac{G_{L1}G_{R1}}{G_{L1}+G_{R1}}(\mu_R-\mu_L)+\left[(G_{L2}+G_{L3})-\frac{G_{L1}(G_{L2}+G_{L3}+G_{R2}+G_{R3})}{G_{L1}+G_{R1}}\right]k\Delta T\right\} \\
&= \frac{em_*A}{2\pi^2\hbar^3}\left\{-\frac{G_{L1}G_{R1}}{G_{L1}+G_{R1}}(\mu_R-\mu_L)+\frac{-G_{L1}G_{R1}}{G_{L1}+G_{R1}}\left[\frac{G_{L2}+G_{L3}}{G_{L1}}-\frac{G_{R2}+G_{R3}}{G_{R1}}\right](-k\Delta T)\right\} \\
&= -\frac{e^2m_*A}{2\pi^2\hbar^3}\frac{G_{L1}G_{R1}}{G_{L1}+G_{R1}}V+\frac{-e^2m_*A}{2\pi^2\hbar^3}\frac{G_{L1}G_{R1}}{G_{L1}+G_{R1}}\left[\frac{G_{L2}+G_{L3}}{G_{L1}}-\frac{G_{R2}+G_{R3}}{G_{R1}}\right]\frac{k}{e}(-\Delta T) \\
&= GV+GS(-\Delta T).
\end{aligned}
$$

$$
\begin{aligned}
J_i &= \frac{m_*A}{2\pi^2\hbar^3}\iint dE_\perp dE_Z(E_Z+E_\perp)\tau_i(E_Z)[f_i(E_Z+E_\perp)-f_C(E_Z+E_\perp)] \\
&= \frac{m_*A}{2\pi^2\hbar^3}\int dE_Z\tau_i(E_Z)\{E_ZkT_i\log[1+e^{(\mu_i-E_Z)/kT_i}]-E_ZkT_C\log[1+e^{(\mu_C-E_Z)/kT_C}]\} \\
&\quad +\frac{m_*A}{2\pi^2\hbar^3}\int dE_Z\tau_i(E_Z)\{(kT_i)^2[-Li_2(-e^{(\mu_i-E_Z)/kT_i})]-(kT_C)^2[-Li_2(-e^{(\mu_C-E_Z)/kT_C})]\} \\
&\approx \frac{m_*A}{2\pi^2\hbar^3}\left\{\int dE_Z\tau_i(E_Z)\frac{(E_Z/kT)^2}{1+e^{E_Z/kT}}k^2T(T_i-T_C)+\int dE_Z\tau_i(E_Z)\log(1+e^{-E_Z/kT})k^2T(T_i-T_C)\right. \\
&\quad \left.+\int dE_Z\tau_i(E_Z)\frac{E_Z/kT}{1+e^{E_Z/kT}}kT(\mu_i-\mu_C)\right\}+\frac{m_*A}{2\pi^2\hbar^3}\left\{\int dE_Z\tau_i(E_Z)\frac{E_Z}{kT}\log(1+e^{-E_Z/kT})k^2T(T_i-T_C)\right. \\
&\quad \left.-2\int dE_Z\tau_i(E_Z)Li_2(-e^{-E_Z/kT})k^2T(T_i-T_C)+\int dE_Z\tau_i(E_Z)\log(1+e^{-E_Z/kT})kT(\mu_i-\mu_C)\right\} \\
&= \frac{m_*A}{2\pi^2\hbar^3}[(G_{i2}+G_{i3})kT(\mu_i-\mu_C)+(G_{i4}+2G_{i5}-2G_{i6})k^2T(T_i-T_C)].
\end{aligned}
$$

$$
\begin{aligned}
J &= -J_L-J_R = \frac{m_*A}{2\pi^2\hbar^3}[(G_{L2}+G_{L3})(\mu_C-\mu_L)kT+(G_{R2}+G_{R3})(\mu_C-\mu_R)kT \\
&\quad +(G_{L4}+2G_{L5}-2G_{L6})k^2T(-\Delta T)+(G_{R4}+2G_{R5}-2G_{R6})k^2T(-\Delta T)]
\end{aligned}
$$

$$
\begin{aligned}
&= -\frac{e^2 m_* A}{2\pi^2\hbar^3}\frac{G_{L1}G_{R1}}{G_{L1}+G_{R1}}\frac{kT}{e}\left(\frac{G_{R2}+G_{R3}}{G_{R1}}-\frac{G_{L2}+G_{L3}}{G_{L1}}\right)\left[\frac{\mu_R-\mu_L}{e}+\left(\frac{G_{L2}+G_{L3}}{G_{L1}}-\frac{G_{R2}+G_{R3}}{G_{R1}}\right)\frac{k}{e}(-\Delta T)\right]\\
&\quad+\frac{m_* A}{2\pi^2\hbar^3}k^2T\left\{-\left[\frac{(G_{L2}+G_{L3})^2}{G_{L1}}+\frac{(G_{R2}+G_{R3})^2}{G_{R1}}\right]+(G_{L4}+2G_{L5}-2G_{L6}+G_{R4}+2G_{R5}-2G_{R6})\right\}(-\Delta T)\\
&= G\Pi(V-S\Delta T)+K(-\Delta T)\\
&= G\Pi V+(K+GS\Pi)(-\Delta T)\\
&= \Pi I+K(-\Delta T).
\end{aligned}
$$

[1] G. Benenti, G. Casati, K. Saito, and R. S. Whitney, Phys. Rep. **694**, 1 (2017).
[2] B. Sothmann, R. Sánchez, and A. N. Jordan, Nanotechnology **26**, 032001 (2015).
[3] H. L. Edwards, Q. Niu, and A. L. De Lozanne, Appl. Phys. Lett. **63**, 1815 (1993).
[4] H. L. Edwards, Q. Niu, G. A. Georgakis, and A. L. De Lozanne, Phys. Rev. B **52**, 5714 (1995).
[5] J. R. Prance, C. G. Smith, J. P. Griffiths, S. J. Chorley, D. Anderson, G. A. C. Jones, I. Farrer, and D. A. Ritchie, Phys. Rev. Lett. **102**, 146602 (2009).
[6] A. N. Jordan, B. Sothmann, R. Sánchez, and M. Büttiker, Phys. Rev. B **87**, 075312 (2013).
[7] S. Kano and M. Fujii, Nanotechnology **28**, 095403 (2017).
[8] B. Sothmann, R Sánchez, A. N. Jordan, and M Büttiker, New J. Phys. **15**, 095021 (2013).
[9] Y. Choi and A. N. Jordan, Phys. E (Amsterdam, Neth.) **74**, 465 (2015).
[10] H. Su, Z. C. Shi, and J. Z. He, Chin. Phys. Lett. **32**, 100501 (2015).
[11] G. Su, Y. Zhang, L. Cai, S. Su, and J. Chen, Energy **90**, 1842 (2015).
[12] S. Su, Y. Zhang, J. Chen, and M. T. Shih, Sci. Rep. **6**, 21425 (2016).
[13] G. Su, T. Liao, L. Chen, and J. Chen, Energy **101**, 421 (2016).
[14] R. Sánchez and M. Büttiker, Phys. Rev. B **83**, 085428 (2011).
[15] Y. Zhang, G. Lin, and J. Chen, Phys. Rev. E **91**, 052118 (2015).
[16] Y. Zhang, C. Huang, J. Wang, G. Lin, and J. Chen, Energy **85**, 200 (2015).
[17] Y. Zhang, Y. Wang, C. Huang, G. Lin, and J. Chen, Energy **95**, 593 (2016).
[18] R. S. Whitney, R. Sánchez, F. Haupt, and J. Splettstoesser, Phys. E (Amsterdam, Neth.) **75**, 257 (2016).
[19] J. S. Lim, D. Sánchez, and R. López, New J. Phys. **20**, 023038 (2018).
[20] A.-M. Daré and P. Lombardo, Phys. Rev. B **96**, 115414 (2017).
[21] H. Thierschmann, R. Sanchez, B. Sothmann, F. Arnold, C. Heyn, W. Hansen, H. Buhmann, and L. W. Molenkamp, Nat. Nanotechnol. **10**, 854 (2015).
[22] B. Roche, P. Roulleau, T. Jullien, Y. Jompol, I. Farrer, D. A. Ritchie, and D. C. Glattli, Nat. Commun. **6**, 6738 (2015).
[23] F. Hartmann, P. Pfeffer, S. Höfling, M. Kamp, and L. Worschech, Phys. Rev. Lett. **114**, 146805 (2015).
[24] M. Josefsson, A. Svilans, A. Burke, E. Hoffmann, S. Fahlvik, C. Thelander, M. Leijnse, and H. Linke, Nat. Nanotechnol. **13**, 920 (2018).
[25] A. J. Keller, J. S. Lim, D Sánchez, R López, S. Amasha, and J. A. Katine, Phys. Rev. Lett. **117**, 066602 (2016).
[26] Z. C. Shi, J. Fu, W. F. Qin, and J. Z. He, Chin. Phys. Lett. **34**, 110501 (2017).
[27] J. H. Jiang, O Entin-Wohlman, and Y. Imry, Phys. Rev. B **85**, 075412 (2012).
[28] J. H. Jiang, O Entin-Wohlman, and Y. Imry, New J. Phys. **15**, 075021 (2013).
[29] C. Li, Y. Zhang, and J. He, Chin. Phys. Lett. **30**, 100501 (2013).
[30] R. Q. Wang, J. C. Lu, C. Wang, and J. H. Jiang, Sci. Rep. **8**, 2607 (2018).
[31] B. Sothmann and M. Büttiker, Europhys. Lett. **99**, 27001 (2012).
[32] B. Rutten, M. Esposito, and B. Cleuren, Phys. Rev. B **80**, 235122 (2009).
[33] B. Cleuren, B. Rutten, and C. Van den Broeck, Phys. Rev. Lett. **108**, 120603 (2012).
[34] Z. C. Shi, J. Z. He, and Y. L. Xiao, Sci. China: Phys., Mech. Astron. **45**, 50502 (2015) (in Chinese).
[35] C. Li, Y. Zhang, J. Wang, and J. He, Phys. Rev. E **88**, 062120 (2013).
[36] J. Wang, Y. Lai, Z. Ye, J. He, Y. Ma, and Q. Liao, Phys. Rev. E **91**, 050102(R) (2015).